Enhancing Oxygen Evolution Reaction Electrocatalytic Performance with Chromium-Doped $LaCoO_3$ Perovskite: Impact of B-Site Doping on Morphology, Structure, and Activity

Elham Fattahi[1], Elham Mahmoudi[2], Elnaz Asghari[3], Ali Coruh[4], Aligholi niaei[5,*]
[1] Department of Chemical & Petroleum Engineering, Tabriz University, Tabriz, Iran
[2] Department of Chemical & Petroleum Engineering, Tabriz University, Tabriz, Iran
[3] Department of Physical Chemistry, Faculty of Chemistry, Tabriz University, Tabriz, Iran
[4] Department of Physics, Sakarya University, Sakarya, Turkey
[5] Department of Chemical & Petroleum Engineering, Tabriz University, Tabriz, Iran and Department of Physics, Sakarya University, Sakarya, Turkey

ABSTRACT

The development of effective and stable electrocatalysts for the oxygen evolution reaction (OER) in an alkaline environment , which can achieve high current density and low overpotential, is a critical challenge. In recent years, perovskite oxides have emerged as promising candidates for efficient OER electrocatalysts due to their versatile physicochemical properties. However, they face certain limitations that hinder their widespread adoption. One approach to improve the electrochemical performance of perovskite oxides is through partial doping of their B-site elements. In this study, we investigated the effect of partial chromium doping on $LaCoO_3$ perovskite, resulting in the formation of $LaCo_{0.5}Cr_{0.5}O_3$. Our results revealed that this compound exhibited outstanding electrochemical activity, with an overpotential of 291.96 mV at a current density of 10 mA/cm^2 and by remaining stable during 4 hours of testing. This improvement was attributed to the increased oxygen vacancy and porosity in the structure of $LaCo_{0.5}Cr_{0.5}O_3$. This study demonstrates that partial substitution in perovskites is an effective means to improve their catalytic activity in the OER process. Furthermore, this strategy can be extended to other perovskite oxides with chromium incorporated into their B-site, potentially resulting in improved performance.

Keywords: Perovskite oxide, Oxygen evolution reaction, Partial doping, Electrochemical activity, Alkaline water electrolysis.

1. INTRODUCTION

The increasing global population and the aspirations of of developing countries to enhance their quality of life have resulted in a surge in energy demand. This has led to two major challenges : (1) the depletion of finite fossil fuels reserves, and (2) the adverse environmental impact of fossil fuel use and combustion. Therefore, transitioning to a sustainable energy future is imperative [1]. Hydrogen, with a high energy density and zero- emission profile upon oxidation, is a promising clean fuel for the future. However, current hydrogen production methods based on fossil fuels, while well-established and cost-effective, are not aligned with the clean energy vision due to their greenhouse gas emissions [2,3]. Water, a ubiquitous and renewable source, is an ideal source of hydrogen that is unaffected by geopolitical considerations. Several methods exist for extracting hydrogen from water, including thermochemical, photoelectrochemical, and electrolytic [4]. Alkaline water electrolysis, in particular, is a cost-effective and straightforward approach for large-scale industrial hydrogen production. One of the key advantages of alkaline electrolyzers is their use of abundant and inexpensive materials, as well as their ability to operate at lower temperatures compared to other electrolysis technologies. Despite its many benefits, alkaline water electrolysis is hinderd by several limitations, including low current density, high overpotential, and consequently, reduced efficiency [5–9].

this process involves two half-reactions: Hydrogen Evoluation Reaction (HER) at the cathode and Oxygen Evolution Reaction (OER) at the anode. OER, requiring four electrons transfer, is the rate-limiting step with the highest overpotential. while, IrO_2 and RuO_2 are highly efficient OER electrocatalysts, their high cost, low durability, and scarcity, it imperative to discover alternative electrocatalysts that exhibit superior OER performance while being cost-effective, abundant, and stable in alkaline environments [10]. Perovskite oxides, characterized by the general formula ABO_3, where A and B represent cations of alkali metals and alkaline earth metals, respectively, have garnered significant interest as potential OER electrocatalysts [11]; as illustrated in Fig 1.

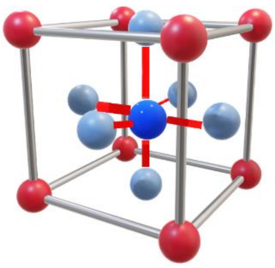

Fig 1. *The structure of ABO3 perovskite oxide (where A is a rare earth or an alkali, red; B is a transition metal, Navy blue; and O is oxygen, light blue)* [11].

Perovskite materials have emerged as potential candidates for efficient OER electrocatalysts in alkaline water electrolysis electrocatalysts because due to their desirable electrical conductivity, abundant constituent elements, and cost-effectiveness. Doping of different elements into the A and B sites of perovskite has been shown to enhance their performance [12,13]. This study aimed to investigate the impact of chromium doping on the OER performance of LaCoO3 perovskite in an alkaline environment. Various structural techniques, including XRD, SEM, EDS, elemental mapping, and FT-IR were utilized to characterize the structure and morphology of the catalysts. In addition, LSV, EIS, and stability analyses were performed to assess the electrochemical performance of Cr-doped $LaCoO_3$ perovskite.

2. MATERIAL AND METHODS

2.1 Reagents and Electrocatalyst Preparation

The chemicals that were used in the synthesis are $Co(NO_3)_2$ .6 H_2O (97%, Merck Company), Glycine (99%, Samchun), $La(NO_3)_3.6H_2O$ (98%, Samchun) and $Cr(NO_3)_3$ .9 H_2O (98%, Samchun). The sol-gel method was utilized to synthesize the perovskite oxides [10]. Firstly, 50 mL of deionized water was heated up to 60 °C on a magnetic heater-strirrer. Then, the nitrate salts of the metals were added while strirring and heating. After reaching to 80 °C, glycine (as the combustion agent) was added with a 1:4 molar ratio of perovskite to glycine. The heating and stirring procedures were continued for approximately 2hr until a gel formed .Subsequently, the gel was treated in an oven at a temperature of 400 °C until combustion occurred. The resulting powders were then calcinated at 700 °C for 6 hours, resulting in the formation of desired perovskites.

2.2 Structural Characterization of Electrocatalysts

To analyze the crystal structure and phase composition, X-ray diffraction using copper Ka radiation (-1.5406) was performed (Tongda TD-3700 China). Further insights into the structure were obtained through FT-IR analysis (TENSOR 27, Bruker, Germany). Additionally, the morphology and elemental distribution of the samples were examined using a scanning electron microscope (FESEM, MIRA3 FEG-SEM, Tescan, Czech Republic) and energy dispersive X-ray spectroscopy (EDS, MIRA3 FEG-SEM, Tescan, Czech Republic**)**.

2.3 Electrochemical measurement

For the electrochemical measurements, a glassy carbon electrode (GCE) with a surface area of 0.0315 cm^2 was utilized as a working electrode, as shown in Fig 2. The electrocatalyst ink was prepared by adding 5 mg of perovskite material, 5 mg of Vulcan Carbon, and 0.5 mg of PVDF to 0.5 ml of ethanol. Since perovskite oxides have a low surface area and poor electrical conductivity due to the high calcination temperature used during the synthesis process, a carbon substance was added to the ink to address this issue [14]. The electrocatalyst ink was then subjected to ultrasound treatment for 2 h. Subsequently, 3 µL of ink were applied on the surface of GCE and allowed to dry at room temperature for 24 h. The electrocatalyst loading on the electrode was 2 mg/cm^2. The electrochemical measurements were conducted at room temperature and atmospheric pressure using a PGSTAT30 galvanostat potentiostat in a three-electrode setup. The working electrode was dropped GCE, the counter electrode was graphite rod and the reference electrode was an Ag/AgCl (3.5 M KCl). Linear sweep voltammetry (LSV) measurements in 1 M KOH were performed in the potential range of 0.2 to 1.25 V at a scan rate of 10 mV/s. EIS measurements were taken at 1.6 V vs RHE (equation (1)) in the frequency range of 100 kHz to 0.01 Hz amplitude. The chrono-potentiometric profile was acquired using a constant current density of 10 mA/cm^2 to test the stability of the best sample during OER. The overpotential of the OER (η), mass activity (MA), and turnover frequency (TOF) was then calculated through the following equations ((2)-(4)), respectively [15,16].

$$E_{RHE} = E_{appl} + 0.197 + 0.059 * PH \qquad (1)$$

$$\eta\ (V) = E_{RHE}(V) - 1.23\ (V) \qquad (2)$$

$$MA = \frac{J}{m} \qquad (3)$$

$$TOF = \frac{J * S}{4 * n * F} \qquad (4)$$

It is known that pH for 1M KOH is 13 [10]. $\eta\ (V)$ is overpotential, J represents current density (mA/cm^2), m represents electrocatalyst loading density on the electrode (mg/cm^2), F is the Faraday constant (96485 C/mol), S is electrode area (cm^2) and n represents the moles of electrocatalytic sites on the working electrode. Moreover, electrochemical double layer capacitance (C_{dl}) and electrochemical active surface area (ECSA) are also among the parameters that got calculated according to the equations (5), and (6) to further study the catalytic activity of the synthesized materials.

$$C_{dl} = \left[Q_0\left(\left(\frac{1}{Rs} + \frac{1}{Rct}\right)\right)^{1-\alpha}\right]^{\frac{1}{\alpha}} \qquad (5)$$

$$ECSA = \frac{C_{dl}}{C_s} \qquad (6)$$

Q_0 , Rs, Rct and α are obtained by Fitting the EIS analysis results with an equivalent circuit in ZVIEW software, in which Rs represents ohmic resistance of electrolyte and Rct is charge transfer resistance [10,17]. As offered by McCrory C_s=0.04 mF/cm^2 [18].

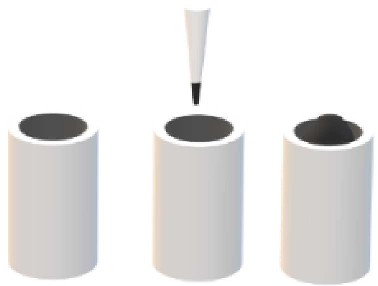

Fig 2. *graphical process of dropping on the working electrode*.

3. RESULTS

3.1 Structure and morphology

The phase and crystal structure of perovskites calcined at 750°C were identified using XRD. The XRD patterns of the synthesized electrocatalysts, as well as the standard cards $LaCoO_3$ (96-412-4853) and $LaCrO_3$ (96-152-6179) associated with these diffractions, were depicted in Fig 3, indicating the successful formation of the target materials. The highly crystalline nature of the samples, especially the chromium-doped sample, was evident from the strong diffraction peaks. By matching the XRDs with the standard card, it was deduced that $LaCoO_3$ and $LaCo_{0.5}Cr_{0.5}O_3$ belong to the space group of Pm-3m and R-3c, respectively. The cubic phase structure was observed for $LaCoO_3$, while $LaCo_{0.5}Cr_{0.5}O_3$ exhibited a hexagonal structure. The intensity of the diffraction peak increased with the increase of chromium content. The LaCoO3 sample exhibited the highest peak at 33˚, whereas the $LaCo_{0.5}Cr_{0.5}O_3$ sample had a peak at 32.68˚ that was slightly shifted to lower angles. This shift can be attributed to Cr^{+3} greater ionic radius (0.129 nm for metallic Cr^{+0}, 0.0615 nm for Cr^{+3}, 0.055 nm for Cr^{+4} and 0.044 nm for Cr^{+6}) compared to Co (0.074 nm for Co^{2+} and 0.061 nm for Co^{3+}) [19]. The partial substitution of the chromium in site B led to structural expansion in sample $LaCo_{0.5}Cr_{0.5}O_3$, causing a minor shift to the left in the XRD pattern. While, Cr substitution may have influenced the oxidation state of cobalt, subsequently affecting the lattice parameters. This leftward shift due to the partial substitution in the perovskite structure can be explained by a significant crystal structure distortion resulting from increased lattice distortion and the Jahn-Teller effect [20]. The structural distortion generates structural defects, particularly oxygen vacancies in the perovskite structure, which are the primary factors in enhancing the OER activity. Therefore, the $LaCo_{0.5}Cr_{0.5}O_3$ sample is anticipated to exhibit superior electrochemical performance as an OER electrocatalyst due to its increased oxygen vacancy concentration, resulting from the aforementioned structural distortion.

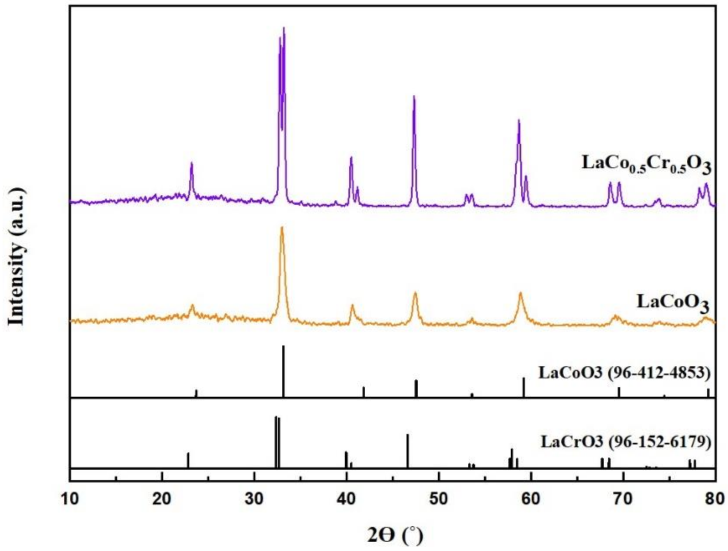

Fig 3. *X-ray diffraction patterns of electrocatalysts.*

FT-IR spectroscopy is an essential technique for determining the chemical composition of synthesized substances. The peaks obtained from the FT-IR spectra of the samples can provide insights into the perovskite structure and its constituent elements. Fig 4 displays the FT-IR spectra of the synthesized perovskite samples in the frequency range of 400-4000 cm^{-1}. Both samples exhibit similar transmission spectra, with prominent bands in the 400-700 cm^{-1} range, indicative of symmetrical and asymmetric B-O stretching in the BO6 octahedral, confirming the formation of the ABO_3 perovskite structure [21,22]. The peaks detected at 450-500 cm^{-1} region correspond to the stretching vibration of the Cr-O bond in the octahedral (Co/Cr)O6 in perovskite oxide compounds[19]. Additionally, peaks detected in the 530-600 cm^{-1} range in the $LaCo_{0.5}Cr_{0.5}O_3$ sample suggest the bending vibration of the O-Cr-O bond. Two minor absorption peaks at approximately 2850 and 2920 cm^{-1} correspond to the symmetric and asymmetric stretching of C-C bonds. The two peaks detected between 1500-1650 cm^{-1} can be attributed to the vibrations of the different oxidation states of Co/Cr (Co^{2+}/ Cr^{2+}, Co^{3+}/ Cr^{3+}) with O (Co-O/ Cr-O) [23]. The bands near 3400 cm^{-1} signify the stretching mode of the hydroxyl functional group (O-H), indicating the presence of adsorbed water on the sample's surface, also observable at 1640 cm^{-1} [22]. The incorporation of chromium in the $LaCo_{0.5}Cr_{0.5}O_3$ perovskite's structure causes a shift of the bands towards higher wavelengths, especially in the 1500 and 1640 cm^{-1} peak region. This shift can be attributed to the difference in ionic radius and atomic mass between Cr and Co atoms, which affects the vibrational frequencies of the sample's constituent elements.

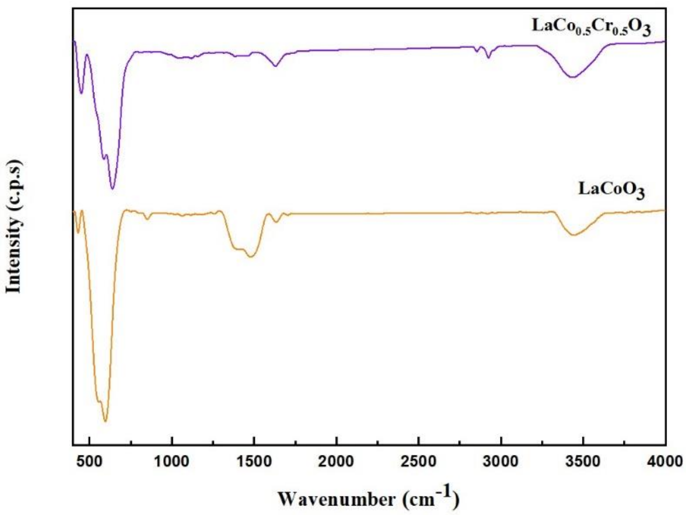

Fig 4. *FT-IR spectra of samples in the wavenumber region of 400–4000 cm^{-1}.*

The morphology of the materials was evaluated using a scanning electron microscope (SEM) at 500 nm and 5 µm magnifications. The results of the SEM analysis revealed that the synthesized perovskite powders primarily consisted of nanoparticles ranging in size from 27 to 195 nm. Compared to $LaCoO_3$, the $LaCo_{0.5}Cr_{0.5}O_3$ perovskite exhibited a more uniform distribution and a more porous structure. The increased porosity of the perovskites can facilitate the diffusion of reactants and products, while also providing a larger active area for electrochemical reactions. Therefore, it is anticipated that the $LaCo_{0.5}Cr_{0.5}O_3$ perovskite will display superior electrochemical performance compared to $LaCoO_3$ due to its improved structural properties.

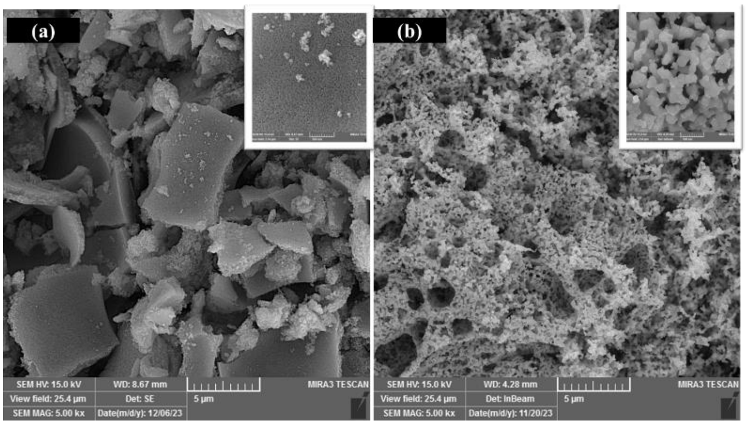

Fig 5. *Surface morphology of a) $LaCoO_3$ and b) $LaCo_{0.5}Cr_{0.5}O_3$ as revealed by SEM imaging.*

The results of elemental mapping and energy dispersive EDX ray analysis are shown in Fig 6. The uniform distribution of La, Co, Cr, and O elements on the surface of the synthesized perovskites is evident from the elemental mapping analysis in Fig 6 (a and c). Furthermore, the EDX results in Figure 6 (b and d) reveal that the molar ratios of La, Co, Cr, and O in both $LaCoO_3$ and $LaCo_{0.5}Cr_{0.5}O_3$ samples are consistent with the theoretical values, confirming the success of the synthesis process. Notably, aside from the peaks corresponding to the constituent elements, some additional peaks are observed in the EDX spectra. These peaks can be attributed to the gold coating applied to the samples surface to enhance their conductivity, which is necessary for obtaining clear images in EDX analysis [21]. Moreover, the Co atomic percentage, which was 22.15 % in the $LaCoO_3$ sample, decreased with increasing chromium doping, reaching 9.64 % in the $LaCo_{0.5}Cr_{0.5}O_3$ sample. This result confirms that chromium has been successfully incorporated into the crystal structure of the perovskite.

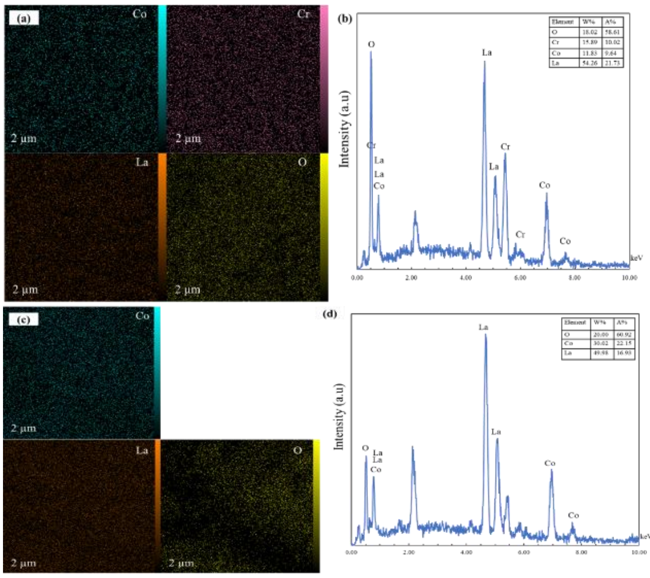

Fig 6. *The elemental mapping patterns of (a) $LaCo_{0.5}Cr_{0.5}O_3$, (c) $LaCoO_3$; EDX spectrum of (b) $LaCo_{0.5}Cr_{0.5}O_3$, (d) $LaCoO_3$.*

3.2 Electrochemical performance

The performance of $LaCoO_3$ and $LaCo_{0.5}Cr_{0.5}O_3$ was evaluated through LSV measurements. Both perovskites demonstrated superior electrochemical activity compared to a bare GC electrode, as evidenced by higher current densities and lower overpotentials(Fig. 7a). Notably, $LaCo_{0.5}Cr_{0.5}O_3$ outperformed $LaCoO_3$ in terms of current density. Fig 7 (b) illustrates the required overpotential for each perovskites to achieve a current density of10 $mA.cm^{-2}$. The incorporation of Cr into the perovskite structure not only enhanced the current density but also positively impacted the electrocatalyst activity by reducing the overpotential from 446.12 mV to 291.96 mV. This improvement can be attributed to an increased number of surface oxygen vacancies [10]. In comparison, IrO2 and RuO2 exhibited overpotentials of 430 and 350 mV, respectively, under similar experimental conditions [24,25]. In addition, the onset potential of $LaCoO_3$ perovskite was found to decrease from 1.53 to 1.48 for $LaCo_{0.5}Cr_{0.5}O_3$, suggesting that LaCoCro3 initiates electrochemical activity more quickly. The Tafel plot, which plots the overpotential against the logarithm of the current density, is a valuable tool for analyzing the OER reaction kinetics of catalysts. As depicted in Fig 7 (c), both perovskites exhibited a lower Tafel slope than bare GC electrode, with $LaCo_{0.5}Cr_{0.5}O_3$ exhibiting the lowest Tafel slope of 125 mV/dec, indicative of its faster reaction kinetic towards OER. Fig. 7d demonstrates that $LaCo_{0.5}Cr_{0.5}O_3$ electrocatalyst exhibits significantly higher mass activity than LaCoO3, highlighting the positive impact of chromium doping on OER performance. Moreover, the TOF values for both perovskites were calculated using equation 4 and found to be 0.0043 1/hr for $LaCoO_3$ and 0.035 1/hr for $LaCo_{0.5}Cr_{0.5}O_3$. These results suggest that $LaCo_{0.5}Cr_{0.5}O_3$ electrocatalyst catalyzes the reaction at a faster rate. It is worth noting that these values were calculated at v=1.583 V vs RHE.

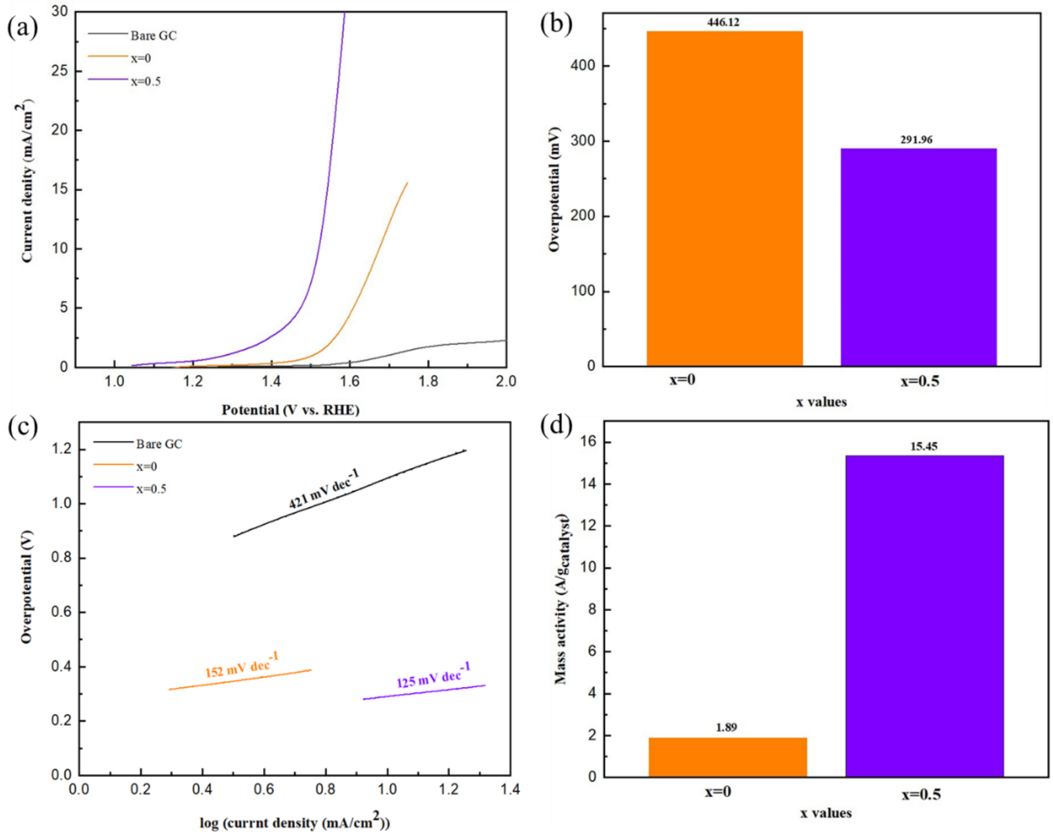

Fig 7. *a) polaization curves b) overpotential values c) Tafel slope plots and d) Mass activity values for* $LaCo_{0.5}Cr_{0.5}O_3$ *and* $LaCoO_3$.

To further investigate the electrochemical performance of the samples, impedance analysis was conducted at 0.6 V vs RHE, and the results, along with the equivalent circuit, are depicted in Fig 8 (a). The smaller semicircle diameter observed for $LaCo_{0.5}Cr_{0.5}O_3$ indicates a lower charge transfer resistance (Rct) compared to $LaCoO_3$, which is advantageous for superior OER electrocatalysis. The decreased electron transfer resistance can be attributed to the porous structure of $LaCo_{0.5}Cr_{0.5}O_3$, as observed in the SEM analysis, which facilates rapid electron transfer across the structure. The electrochemical double-layer capacitance (Cdl) of both perovskites was then calculated using the impedance analysis parameters and equation 5. Utilizing this value, the electrochemical active surface capacitance for both samples was determined for both samples (Fig 8 (b)). $LaCo_{0.5}Cr_{0.5}O_3$ displayed a higher Cdl and electrochemical active surface, further supporting its superior electrochemical performance.

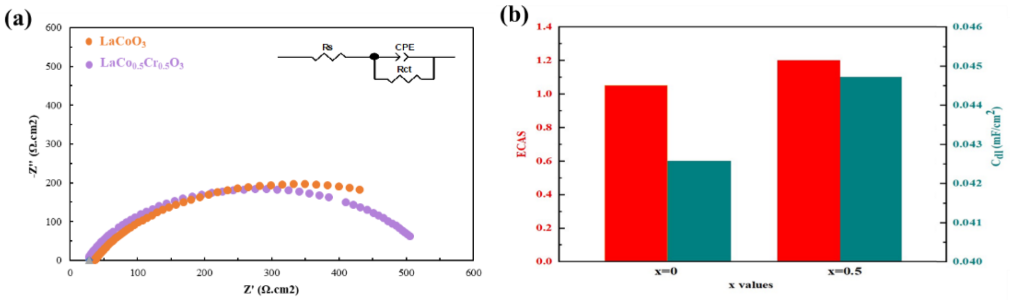

Fig 8. (a) *EIS Nyquist plots (b) ECAS and C_{dl} of $LaCo_{0.5}Cr_{0.5}O_3$ and $LaCoO_3$.*

The electrochemical results thus far have consistently demonstrated that $LaCo_{0.5}Cr_{0.5}O_3$ outperformed its undoped counterpart, $LaCoO_3$, in all tests. To evaluate the stability of $LaCo_{0.5}Cr_{0.5}O_3$, a chronopotentiometry test was conducted at a current density of 10 mA/cm^2, and the results are depicted in Fig. 9. Remarkably, the potential remained almost constant at applied 1.5 V vs RHE throughout the entire test duration of 4 hours, indicating that $LaCo_{0.5}Cr_{0.5}O_3$ is a highly stable electrocatalyst for OER in an alkaline environment. This result is of great significance in practical applications, as it suggests that $LaCo_{0.5}Cr_{0.5}O_3$ can maintain its excellent performance over extended periods of operation, making it a promising candidate for large-scale industrial use.

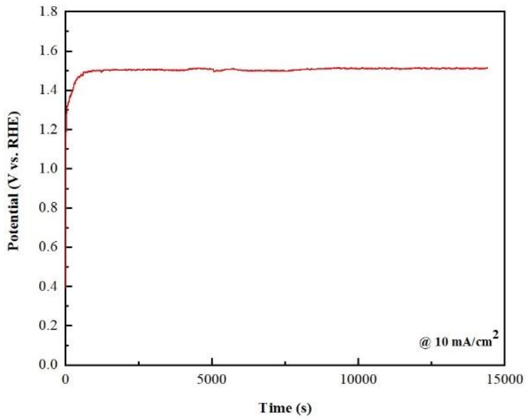

Fig 9. *Stability profile of $LaCo_{0.5}Cr_{0.5}O_3$.*

4. CONCLUSION

In this study, a sol-gel method was used to synthesize two perovskites, $LaCoO_3$ and $LaCo_{0.5}Cr_{0.5}O_3$, with the aim of creating OER electrocatalysts. Based on the structural analysis, it was anticipated that both materials would form successfully. The XRD results indicated that incorporating chromium into $LaCoO_3$ perovskite resulted in structural distortion and may lead to increased oxygen vacancies. SEM investigation further revealed that $LaCo_{0.5}Cr_{0.5}O_3$ had a more porous structure compared to $LaCoO_3$ perovskite. These features, such as possible oxygen deficiency and porosity, , were found to contribute to the enhanced electrochemical activity of the electrocatalysts in OER. $LaCo_{0.5}Cr_{0.5}O_3$ showed an improved catalytic performance with higher current density, lower overpotential, and a lower Tafel slope, as revealed by the assessment of the electrochemical performance of both obtained samples. Furthermore, TOF, MA, Cdl, and ESCA values increased with the addition of Chrome in the $LaCoO_3$ Perskite. To conclusion, the incorporation of chromium on the B-site of perovskites was found to be a promising strategy for enhancing the electrocatalytic performance in OER, making it a potential candidate for applications in renewable energy technologies.

Acknowledgements: The researchers extend their thanks and appreciation to the collaboration and support of the Department of Chemical and Petroleum Engineering, and the Department of chemistry at the University of Tabriz, the Department of Physics at the University of Sakarya and the Scientific and Technological Research Council of Turkey (TUBİTAK).

REFERENCES

[1] T.N. Veziroğlu, S. Şahi, 21st Century's energy: Hydrogen energy system, Energy Convers Manag 49 (2008) 1820–1831.

[2] K. Kamlungsua, P. Su, S.H. Chan, Hydrogen generation using solid oxide electrolysis cells, Fuel Cells 20 (2020) 644–649.

[3] T.E. Lipman, What will power the hydrogen economy? Present and future sources of hydrogen energy, (2004).

[4] D.J. Deka, S. Gunduz, J. Kim, T. Fitzgerald, Y. Shi, A.C. Co, U.S. Ozkan, Hydrogen production from water in a solid oxide electrolysis cell: effect of Ni doping on lanthanum strontium ferrite perovskite cathodes, Ind Eng Chem Res 58 (2019) 22497–22505.

[5] S. Anwar, F. Khan, Y. Zhang, A. Djire, Recent development in electrocatalysts for hydrogen production through water electrolysis, Int J Hydrogen Energy 46 (2021) 32284–32317.

[6] D.D. de Fátima Palhares, L.G.M. Vieira, J.J.R. Damasceno, Hydrogen production by a low-cost electrolyzer developed through the combination of alkaline water electrolysis and solar energy use, Int J Hydrogen Energy 43 (2018) 4265–4275.

[7] K. Zeng, D. Zhang, Recent progress in alkaline water electrolysis for hydrogen production and applications, Prog Energy Combust Sci 36 (2010) 307–326.

[8] J. Chi, H. Yu, Water electrolysis based on renewable energy for hydrogen production, Chinese Journal of Catalysis 39 (2018) 390–394.

[9] N. Guillet, P. Millet, Alkaline water electrolysis, Hydrogen Production: Electrolysis (2015) 117–166.

[10] E. Mahmoudi, J. Mostafaei, C. Griesser, M.F. Bekheet, N. Delibas, S. Penner, E. Asghari, A. Coruh, A. Niaei, LaCoO3-BaCoO3 porous composites as efficient electrocatalyst for oxygen evolution reaction, Chemical Engineering Journal 473 (2023) 144829.

[11] X. Xu, Y. Chen, W. Zhou, Z. Zhu, C. Su, M. Liu, Z. Shao, A perovskite electrocatalyst for efficient hydrogen evolution reaction, Advanced Materials 28 (2016) 6442–6448.

[12] J. Xu, C. Chen, Z. Han, Y. Yang, J. Li, Q. Deng, Recent advances in oxygen electrocatalysts based on perovskite oxides, Nanomaterials 9 (2019) 1161.

[13] E.A.R. Assirey, Perovskite synthesis, properties and their related biochemical and industrial application, Saudi Pharmaceutical Journal 27 (2019) 817–829.

[14] M. Zhang, G. Jeerh, P. Zou, R. Lan, M. Wang, H. Wang, S. Tao, Recent development of perovskite oxide-based electrocatalysts and their applications in low to intermediate temperature electrochemical devices, Materials Today 49 (2021) 351–377.

[15] H. Jia, Y. Yao, J. Zhao, Y. Gao, Z. Luo, P. Du, A novel two-dimensional nickel phthalocyanine-based metal–organic framework for highly efficient water oxidation catalysis, J Mater Chem A Mater 6 (2018) 1188–1195.

[16] Z. Wu, X.F. Lu, S. Zang, X.W. Lou, Non-noble-metal-based electrocatalysts toward the oxygen evolution reaction, Adv Funct Mater 30 (2020) 1910274.

[17] C.C.L. McCrory, S. Jung, J.C. Peters, T.F. Jaramillo, Benchmarking heterogeneous electrocatalysts for the oxygen evolution reaction, J Am Chem Soc 135 (2013) 16977–16987.

[18] C.C. Wang, Y. Cheng, E. Ianni, B. Lin, A highly active and stable La0. 5Sr0. 5Ni0. 4Fe0. 6O3-δ perovskite electrocatalyst for oxygen evolution reaction in alkaline media, Electrochim Acta 246 (2017) 997–1003.

[19] M. Coskun, O. Polat, F.M. Coskun, Z. Durmus, M. Caglar, A. Turut, Synthesis, characterization and wide range frequency and temperature dependent electrical modulus study of LaCrO3 and cobalt (Co) doped LaCrO3 perovskite compounds, Materials Science and Engineering: B 248 (2019) 114410.

[20] X. Lang, H. Mo, X. Hu, H. Tian, Supercapacitor performance of perovskite La 1− x Sr x MnO 3, Dalton Transactions 46 (2017) 13720–13730.

[21] N. Zarrin, S. Husain, W. Khan, S. Manzoor, Sol-gel derived cobalt doped LaCrO3: structure and physical properties, J Alloys Compd 784 (2019) 541–555.

[22] M. Ahangari, J. Mostafaei, H. Zakerifar, A. Sayyah, N. Delibaş, A. Çoruh, E. Mahmoudi, E. Asghari, A. Niaei, Effect of Pd doping on the structural properties and supercapacitor performance of La0. 8Sr0. 2Cu0. 7Mn0. 3O3 and La0. 8Sr0. 2Cu0. 4Mn0. 6O3 as electrode materials, Electrochim Acta 470 (2023) 143274.

[23] M. Ahangari, J. Mostafaei, A. Sayyah, E. Mahmoudi, E. Asghari, A. Coruh, N. Delibas, A. Niaei, Investigation of structural and electrochemical properties of SrFexCo1-xO3-δ perovskite oxides as a supercapacitor electrode material, J Energy Storage 63 (2023) 107034.

[24] J. Wang, Y. Gao, D. Chen, J. Liu, Z. Zhang, Z. Shao, F. Ciucci, Water splitting with an enhanced bifunctional double perovskite, ACS Catal 8 (2018) 364–371.

[25] J. Yu, X. Wu, D. Guan, Z. Hu, S.-C. Weng, H. Sun, Y. Song, R. Ran, W. Zhou, M. Ni, Monoclinic SrIrO3: an easily synthesized conductive perovskite oxide with outstanding performance for overall water splitting in alkaline solution, Chemistry of Materials 32 (2020) 4509–4517.